Lasers in Manufacturing Conference 2017

Perspectives of laser-beam welding of ultra-high steels

Martin Dahmen[a,*], Stefan Lindner[b], Dirk Petring[a]

[a]*Fraunhofer-Institute for Laser Technology, Steinbachstraße 15, 52074 Aachen, Germany*
[b]*Outokumpu Nirosta GmbH, Oberschlesienstraße 16, 47807 Krefeld, Germany*

Abstract

The increasing demand for sustainable manufacturing in sheet metal processing and vehicle manufacturing led to the application of new alloys with ultra-high strength and increased ductility. Due to strengths of up to 2 GPa in martensitic steels or the increase of strength by twinning in high-manganese steels mechanical joining is not possible. Fusion welding is an option where the limitation of energy input leads to the application of laser beam welding as the joining technology in this class of materials. Investigations on welding similar and dissimilar joints of martensitic stainless steel and a stainless high-manganese steel and a variety of different steel grades, respectively, were undertaken. Contradictory demands on the conduct of the welding process were revealed. Martensitic steels require a heat treatment whereas the TWIP steels react positively on a mechanical treatment. Especially in dissimilar welds effects of the gauge length, the strength of the individual partners, and local microstructure in the weld caused by intermixing effect determine strength and fracturing of the joints. The contribution gives an overview over the results and shows the potential for the application of laser beam welding for joining in assembly of structural parts.

Keywords: Joining; laser beam welding; ultra-high strength steels; high-manganese steels; mechanical properties; weld metallurgy

1. Introduction

New ultra-high strength steels provide new lightweight opportunities and improve crash properties in future car bodies. By reducing the dead weight payload can be increased in vehicle construction for street and rails. Ultra-high strength steels with excellent deformation properties (Bouaziz et al., 2011) and intrinsic corrosion resistance are now commercially available. In order to utilize them different joining methods can

* Corresponding author. Tel.: +49-241-8906-307; fax: +49-241-8906-121.
E-mail address: martin.dahmen@ilt.fraunhofer.de.

be applied. As mechanical joining methods such as friction stir welding or self-piercing riveting are not applicable due to the high strength of the materials fusion welding should be applied with a strong limitation of the energy input. In the current contribution the effects of laser beam welding shall be investigated. Understanding the joining process as well as the response of the base materials on heat input is in order to create designs exploiting the full potential and fulfil the extensive requirements.

The similar laser-welded TWIP (TWinning Induced Plasticity) steels joints exhibit a dendritic microstructure. Macrographs report a fully austenitic structure with grain coarsening in both, fused zone (FZ) and heat-affected zone (HAZ), where the latter is about 300µm wide (Dahmen, Lindner, Monfort, Petring, 2016). A few publications dealing with the laser welding of TWIP steels to other grades are currently available. The main issue in these dissimilar welds is the appearance of chemical and/or phase inhomogeneities in the FZ since the multistage strain hardening of TWIP steels strongly depends on the composition (Mujica et al., 2009).

The welding suitability of a martensitic stainless steel (1.4034) in as-rolled as well as in press hardened condition and the mechanical properties of welded joints have been reported (Janzen et al. 2015). Fatigue test results were displayed for the case of hot stamped tailored blanks. The fatigue strength of the welded specimen, determined by fatigue tests, amounts to about 44% at $1{\cdot}10^7$ cycles compared with the fatigue strength of the base material. The results indicate a fatigue class of above FAT 100. Quasi-static and dynamic tests according to the KS2 method reflect the behaviour of welds in hardened material for assembly. Load capacity and deformation are comparable to those of manganese boron steels. The scattering of the measurements ranges up to 9%. In all cases the joints failure mode is a brittle fracture in the weld zone. In as-rolled and in press hardened condition high hardness at the fusion line, caused by untempered martensite, requires a tempering treatment. For hot stamping this step can be. After hot stamping the heat-affected zone is transformed completely. Even the segregation lines are restored. A slight decrease of hardness in the former high-temperature heat-affected zone and in the fusion zone indicates the presence of a weld. The weld zone shows an increased content of retained austenite and consequently a decrease in hardness (Dahmen et al. 2015).

As the 1.4034 the grade 1.4678 is a derivative of 1.4301 (304) where nickel is replaced by manganese. The steel is fully austenitic and exhibits strong work hardening by the TWIP effect (Graessel et al., 2000). The original yield strength of 500 MPa can be increased to up to 1100 MPa by cold forming. Material at low and middle strength level show an excellent welding suitability whereas welding becomes difficult at a strength above approximately 800 MPa (Lindner, 2014) The work hardening is lost in the fused zone but can be regained upon deformation (Lindner, Gerhards, Dahmen, 2015a).

Experiments have demonstrated the formation of a martensitic phase in the dissimilar welds of TWIP HSD60 to ferritic S420MC. Depending on the mixing ratio of HSD600 into S420MC, more or less martensite appeared. This shall be explained by the shift of austenitic former concentration into the weld pool. In this study, the most efficient microstructure to be obtained with overlap welds offering maximum shear forces, was that with the largest austenite fraction in the joining plane. This is achieved through full penetration weld, welding from TWIP to S420MC sheet with a speed of 3 mmin-1. It was emphasized that mechanical shear strength of the dissimilar welds was not better than that of the weakest alloy (Behm et al. 2014).

Further studies on dissimilar butt joints TWIP Fe-22Mn-0.6C to a TRIP800 by (Mujica et al. 2010) reported segregation of manganese in the FZ and subsequent martensite formation. Manganese segregations in the form of C-Mn precipitates have also been reported along the dendrite boundaries in a TWIP/TRIP butt joint close to the TWIP side (Rossini et al. 2015). Under tensile load, the latter butt joint fractured in the fusion zone. The resulting dissimilar joints exhibited poor mechanical strength.

2. Experimental details

The austenitic TWIP steel is a new 1.4678 with a manganese content of 16.5 weight percent cold worked to a yield strength of 1 GPa. Partner materials under investigation comprise a metastable austenitic steel 1.4301 (304) and a martensitic stainless steel 1.4034 (420) in press hardened condition, respectively. Table 1 shows the chemical composition of the three materials. All values refer to ladle analyses taken during production of the sheet metal. Sheet thickness is 1.1 mm in the case of the manganese steel, 1.5 and 2 mm for the chromium-nickel and the chromium steel, respectively.

During production the materials have undergone different treatments. The high manganese steel was cold rolled from its initial state at a yield strength of 500 MPa. The microstructure is fully austenitic. Cold rolling with subsequent annealing was applied at the austenitic stainless steel 1.4301. Base for the martensitic steel is a martensitic-ferritic stainless steel produced by cold rolling and annealing. Its microstructure consists of 94% austenite and 6% ferrite. For press hardening sheets were austenitised at 1150 °C, quenched in a die, and tempered at 400 °C for 5 minutes. The resulting microstructure consists of martensite and approximately 28% austenite.

Table 1. Chemical compositions of the steels in weight percent

Material	C	Mn	Si	S	P	Cr
1.4034	0.455	0.52	0.35	0.001	0.025	13.72
1.4301	0.04	1.4	0.5	0.012	0.04	19.1
1.4678	0.30	16.5				14.9

Welds were produced at butt as well as on overlap joints, in the latter case the manganese steel was situated on the top. In order to limit the thermal load on the materials autogenous laser beam welding was applied for joining. All welding was conducted at room temperature with cooling at still air. In order to secure best achievable weld integrity as beam source a CO_2 laser was used. The beam was focused by a mirror of 200 mm focal length onto a focal spot of 340 µm diameter. The welding parameters are listed in Table 2. As assist gas helium at a flow rate of 15 min^{-1} was applied. An argon flow of 20 l min^{-1} was used for root shielding. Specimens were prepared by laser beam fusion cutting of strips of 30×80 mm^2. No post-processing of the edges was applied.

Table 2. Welding parameters

Material	Butt joints	Lap joints		
Experiment No.	1,2,3	4	5	6
Beam power P_L/kW	2,06		2.6	
Focal position Δz/mm		2		
Welding speed v_s/mmmin^{-1}	4	3.8	3.8	2.8
Heat input E_s/kJm^{-1}	31	41	41	56

Weld quality was assessed according to DIN EN ISO 13919-1. No failures were reported for the square butt welds in ultra-high steels. In the manganese steels some solid inclusions were detected. Residuals of the separation agent used during casting are suspected to be the reason. All welds are rated as class B "stringent".

Metallographic inspection was carried out by standard grinding and polishing. Depending on the materials the etching procedure varied and is outlined in the respective paragraphs.

In order to forecast the mechanical properties micro-hardness measurements were at after Vickers at a test load of 1 N were carried out. Strength and fracture behaviour have been tested by tensile tests were at straight specimens with a width of 30 mm according to the definition of SEP 1220 part 3. The specimens were produced by laser beam cutting with non-machined edges. During testing the deformation rate was kept constant at 0.02 mmmin^{-1}.

3. Results

3.1. Similar welds in high manganese steels

The macro section of a square butt weld shown in figure 1a exhibits a dumbbell shaped seam with a width of 0.4 mm at the middle level. As results of the hardness measurements the distribution of indentation hardness is displayed in figure 1b. In case of a similar weld a decrease from average 480 HV0.1 to approximately 300 HV0.1 becomes obvious. This represents the hardness of the solution annealed material. The transition is smooth, no extremal values are measured. This indicates the loss of hardness, and hence, strength, by stress relieving through the welding heat. The total width of the heat-affected zone is indicated to about 0.22 mm.

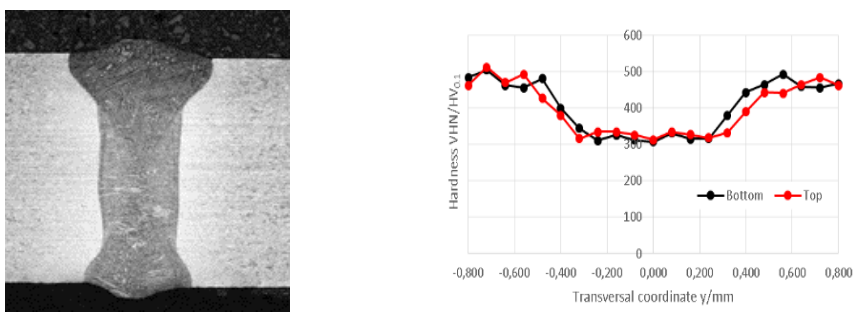

(a) (b)

Fig. 1: Similar square butt weld in 1.4678 (FORTA H1000): (a) Macro section and (b) hardness plot across the weld zone

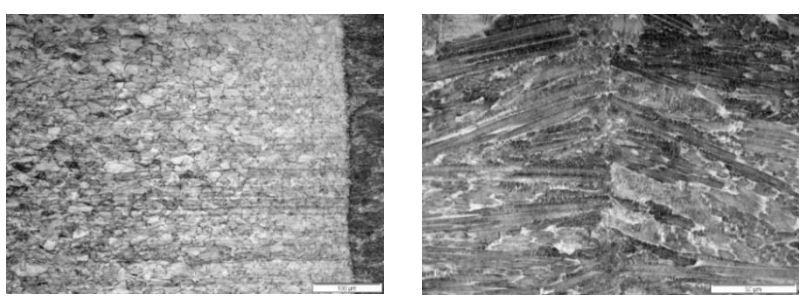

(a) (b)

Fig. 2. Photographic images of the weld microstructures in the 1.4678 similar joint: (a) Heat-affected zone and fusion line (scale 100µm); (b) Weld centre line (scale 50 µm)

In lap weld configuration microstructure and hardness distribution are the same as for square butt joints. Due to the increased energy input for the twin sheet welding the seam at the intersection is about 0.5 mm in width. Hardness is not affected by the energy input and amounts to approximately 320 HV0.1.

Figure 2 shows two micro sections of the similar weld in 1.4678. The heat-affected zone in figure 2a is very small, as a consequence of the low thermal conductivity of the TWIP steel (Lan (2016)). Over a width of 90 µm slight grain refinement can be observed. Approaching the unaffected base material an approximately 100 µm wide zone with grain size equal to the base material, but with the cold working texture resolved follows (figure 2a from right to left). The fused zone is characterized by dendritic solidification (fig. 2b). Its microstructure is fully austenitic. By the etching pattern a slight segregation of manganese at the dendrite boundaries, visible as brighter areas, can be concluded.

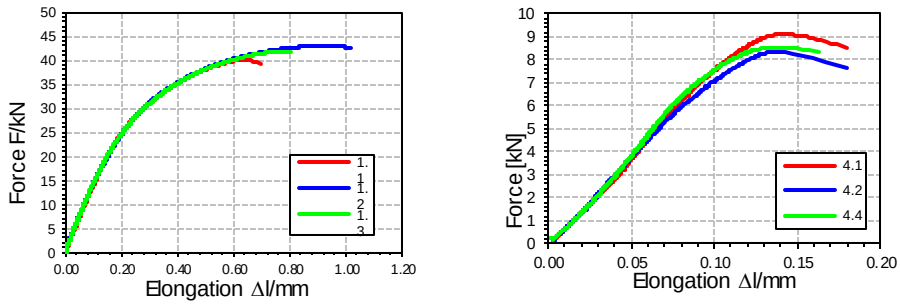

Fig. 3. Tensile test results of a similar square butt weld in high manganese steel: (a) Force-elongation curves from transverse tensile tests, (b) Force-elongation curves from shear tests

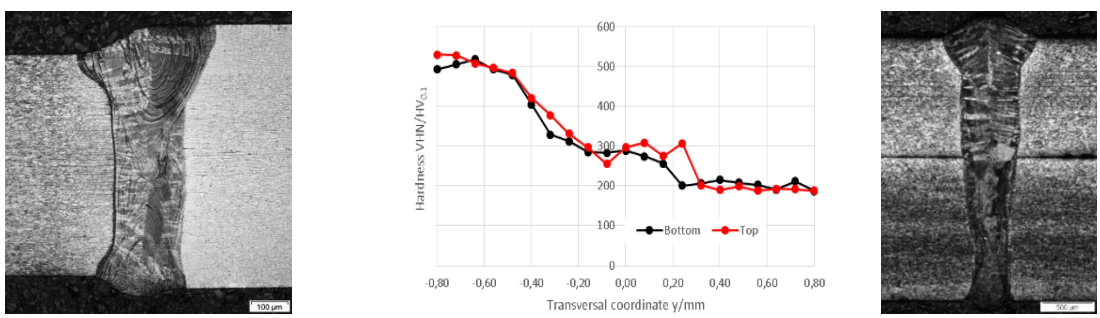

Fig. 4. Dissimilar weld between 1.4678 and 1.4301: (a) Macro section of a square butt joint; (b) hardness plot across the weld zone; macro section of a lap joint

The hardness values and their distribution is reflected in the results of the tensile tests. They show large scattering with respect to the elongation at fracture (figure 3a). In the similar combination 1.4678/1.4678 fracture and full elongation occur in the weld which is the weakest zone as shown by the hardness measurement. The graph in figure 6a show a characteristic curve for high-manganese steels. Yielding starts at approximately 17 kN and fracture occurs at forces above 40 kN. Recalculated yield strength amounts to 552 MPa. Hence, the weld shows the strength of the normalized material. In the case of the red curve the crack initiated at the weld centre line on the edge of the specimen. At the other specimens fracture was initiated at the fusion line and propagated diagonally through the weld to the opposite fusion line. In the shear tests a maximum tensile force of 8.3 to 9 kN was measured (figure 3b). The rise of the curve show a slightly progressive slope caused by the out-of-plane bending of the sheets. At a force of approximately 5 kN the curve becomes degressive, indicating plastic deformation and necking. The engineering stress amounts to 550 MPa.

3.2. Dissimilar welds

3.2.1. Dissimilar welds with austenitic stainless steel

Figure 4 a shows the macro section of a square butt joint between 1.4678 (left) and 1.4301 (right). From the photograph a separation in to zones along the weld centre line becomes obvious. This effect is caused by the shedding of vortices washing up the material from one side to the fusion line on the opposite side. The macro section of the lap joint shown in figure4c shows some mixing streaks at the level of the separation of the sheet caused by vertical mixing.

The hardness distribution of the weld 1.4678 to 1.4301 shows a steady transition from approximately 500 to 200 $HV_{0.1}$ between the materials (figure 4b). In the lap welds an increased hardness of up to 301 HV0.1 was measured, equalling the hardness of the cast or solution treated manganese steel. As consequence the tensile strength will be increased in this region compared to the strength of the 1.4301.

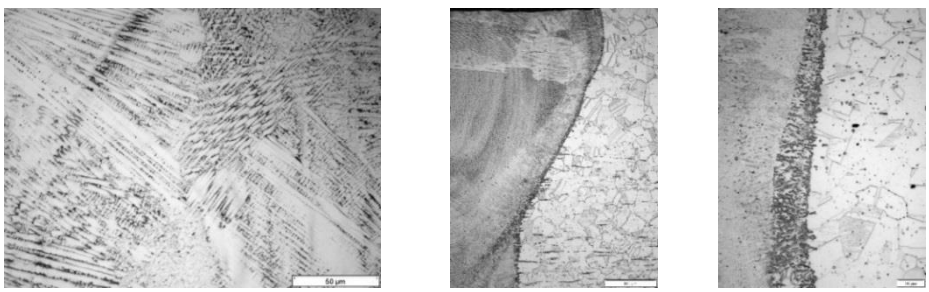

(a) (b) (c)

Fig. 5. Photographic images of the weld microstructures in the 1.4678/1.4301 dissimilar joint: (a) at weld centre line (scale 50 µm); (b) fusion and heat affected zone line at the weld top (scale 100 µm); (c) a detail of the fusion line (scale 20 µm)

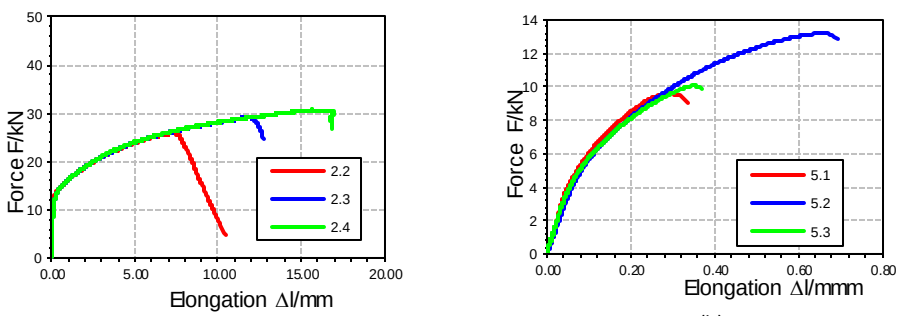

(a) (b)

Fig. 6. Tensile test results of dissimilar joints of 1.4678 and 1.4301: (a) Force-elongation curves from transverse tensile tests, (b) Force-elongation curves from shear tests

Mixing features become obvious in the weld of the combination 1.4678 and 1.4301. A photograph of the microstructure at the weld centre line is shown in figure 5a. Due to the increased carbon content in the mixed material the solidification appears to be columnar with dendritic substructure. In figure 5 b and c details of the microstructure at the fusion line of the 1.4301 are depicted. The microstructure of the fused zone appears fully austenitic. The solidification occurs as columnar with dendritic substructure. Compared to the similar joint, the microstructure has less preferential orientation and the dendrite spacing is smaller. At the fusion line of the 1.4301 (fig. 5b) the equi-axially solidified: unmixed zone is visible. Adjacent in the fused material single alloy carbides segregated at the boundaries of the first layer of columnar crystallites (fig. 5c).

Fracture in the dissimilar weld of 1.4678 and 1.4301 originates at the fusion line of the austenitic stainless steel but deviates soon into the base material forming a ductile crack. All plastic deformation is found here which shows a fracture strain of 25 to 36% and a necking of 10 to 26% in the base material. Yielding starts at 11.5 kN, fracture occurs at above 29 kN. Recalculated tensile strength is minimum 640 MPa, yield strength amounts to 256 MPa. The strength of this weld is defined by the weaker material (figure 6a).

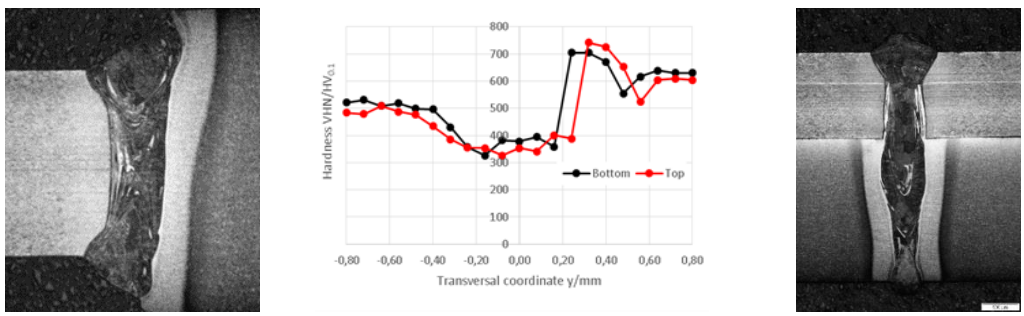

(a) (b) (c)

Fig. 7. Dissimilar weld between 1.4678 and press hardened 1.4034: (a) Macro section of a square butt joint (b) hardness plot across the weld zone; (c) macro section of an overlap joint

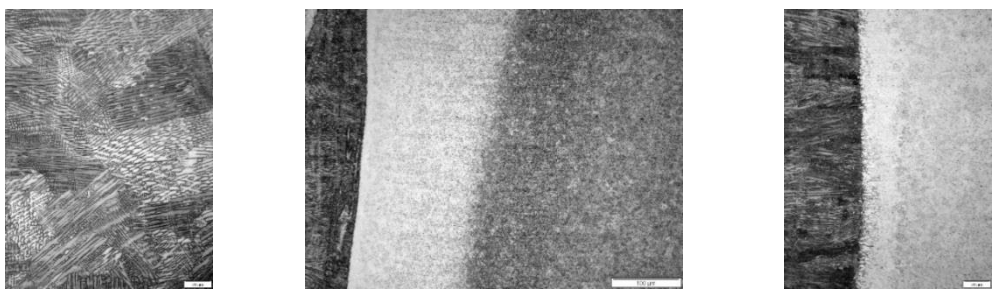

(a) (b) (c)

Fig. 8. Microstructure of the dissimilar weld between 1.4678 and press hardened 1.4034: (a) Weld centre line (scale 20 µm); (b) Heat-affected zone in 1.4034 (scale 100 µm); (c) Fusion line to 1.4034 (scale 20 µm)

The shear test results show a large scattering in the force at fracture, whereas the elastic limit seems to be stable at about 4 kN. The large difference to the fracture force is assumed to a plastic bending of the 1.4301 induced by the out-of-plane introduced load (figure 6b).

3.2.2. Dissimilar welds with press hardened martensitic stainless steel

The macro section in fig. 7a shows the seam shape of a weld connecting a 1.1 mm thick 1.4678 and a 1.5 mm thick sheet of 1.4301. For revealing the microstructure the polished specimen was double etched starting with Adler's reagent followed by electrolytic etching under oxalic acid.

The hardness distribution was measured at a distance of 0.2 mm from the upper and lower surface, respectively, of the thinner sheet. It shows a straight transition from approximately 500 in the 1.4678 to 200 HV0.1 in the 1.4301 between the materials (figure7b).

Figure 8 shows a detail of the microstructure at the weld centre line in a dissimilar weld between 1.4678 and 1.4034. In some of the columnar grains a lath structure is visible indicating martensite. In figure 8b a micrograph of heat-affected zone is shown. Adjacent to the fusion line a bright layer of a width of 12 µm is

observed consisting of untempered martensite. Figure 8c shows a detail of the area around the fusion line. The martensitic area is followed by a region with partially hardened material over a width of 100 µm at the centre and 150 µm at root and upper bead. Between this zone and the base material an area with larger grains indicating an increased content of austenite can be seen in the cross section as darker area. Here a tempering of the hardened base material occurs.

Fracture in the dissimilar weld of 1.4678 and 1.4301 originates at the fusion line of the austenitic stainless steel but deviates soon into the base material forming a ductile crack. All plastic deformation is found here which shows a fracture strain of 25 to 36% and a necking of 10 to 26% in the base material. The red curve is not representative for the peak values because the specimen experienced some slip in the wedged clamps, but shows the same slope until failure. Yielding starts at 11.5 kN, fracture takes place at above 29 kN. Recalculated tensile strength is minimum 640 MPa, yield strength amounts to 256 MPa. The strength of this weld is defined by the weaker material. Failure mainly occurs at the fusion line to the 1.4301, but sometimes also found at the weld centre line (figure 9b).

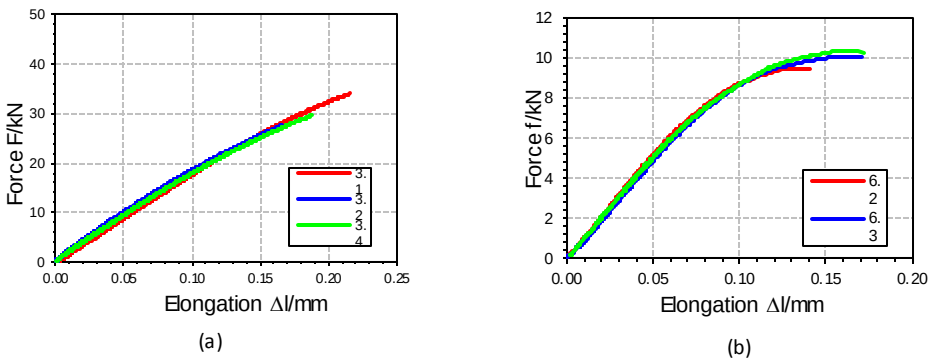

Fig. 9. Tensile test results of dissimilar welds between 1.4678 and 1.4034: (a) Force-elongation curves from transverse tensile tests, (b) Force-elongation curves from shear tests

The shear test results show a fairly consistent behaviour (figure 9b). A tensile force of 9.5 to 10 kN at an elongation to fracture of about 0.15 mm is attained. Bending of the sheets appears to be less pronounced due to the high stiffness caused by the high strength and the thicker martensitic steel sheet. Deformation occurs mainly in the austenitic material. A shear strength of 670 MPa was attained.

4. Weld metallurgy

Figure 10 shows a redrawn Schaeffler diagram considering the phase transformations observed in high manganese steels as developed by Klueh, Masiasz, and Lee, 1988. The original Schaeffler diagram (dashed lines) are superimposed on the modified (solid lines) diagram. The point for the different alloys are symbolised as coloured dots. In the original diagram the grade 1.4678 is found in the fully austenitic region whereas in the modified diagram it should contain some percent of δ-ferrite. For the other two grades the original diagram has to be considered. The indication of 1.4034 is located in the austenitic-martensitic area with some 40% martensite in the as-rolled and 72% in the press hardened condition. The metastable austenitic grade is found in the austenitic-ferritic region with less than 10% ferrite. According to the correction by Lee et al., 2015, the indication if the alloy becomes situated in the austenite region.

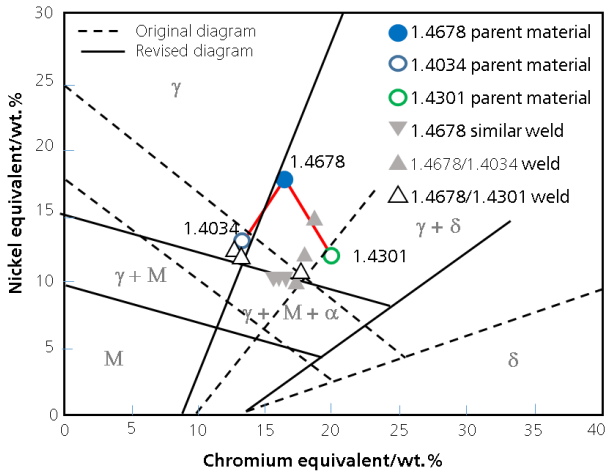

Fig. 10. Alloy composition of the weld metals in the standard and the modified Schaeffler curve with an indication.

As the composition of the fused material is considered to be defined by mixing of both partner materials it is expected their indication lies on the connecting lines. Table 3 lists the results from local EDS measurements, the figures are symbolised by triangles in the Schaeffler diagram in figure 10. There is, depending on the local mixing situation, a wide variation of alloying elements. Recalculation from the EDS measurements using the nickel and chromium equivalents show approximately the same trend. In the similar joints the actual composition shifts the phase distribution towards the ferritic and martensitic region (grey triangles upside down). For the grade 1.4678 welds with the partner 1.4301(upright grey triangles) the structure predicted can contain up to 10% δ-ferrite and also traces of martensite. The decrease in nickel equivalent can be caused by the loss of manganese which can amount to up to 2% (Dahmen, Daamen, Hirt, 2014) or by dilution. Nickel suppresses the formation of martensite but may occasionally lead to the segregation of carbides. In the weld to 1.4034 (white triangles) two measuring areas show a similar composition as the base material but shifted to the martensite region. Mixing with the manganese steel leads in one case to a structure containing austenite and ferrite. During metallographic inspection austenite was the dominating phase, in conjunction with 1.4034 also streaks with martensitic structure occurred.

The scattering of the tensile results of the tensile tests for the combination 1.4678/1.4034 are - hypothetically - caused by the discontinuous structure of the heat-affected zone. The presence of untempered body-centred tetragonal martensite introduces stresses and may lead to cold cracking. Heat treatment of the weld can especially improve the properties of the martensitic stainless steel. Pre-heating to martensite start temperature in conjunction with tempering at 400 °C was beneficial in order to improve the fatigue properties. The reaction of the austenitic high-manganese steel and especially its strength on such a heat treatment is currently not known. Mazancová, Ružiak, and Schindler, 2012, have proven that high manganese steel Fe-0.18C-28Mn-2.3Al-0.98Si tolerates a heat treatment at 500 °C for one hour without loss of hardness. At a dwell time of six minutes an increase in hardness was observed which disappeared on longer holding. For the actual alloy of 1.4678 in cold worked state dedicated experiments still have to be conducted.

In order to understand the complex nature of fracture in the combination with the press hardened martensitic stainless steel a critical evaluation of the failure mode is required. This has to be done by meticulous metallographic inspection, fracture analysis and considerations of fracture mechanics. In this frame also the effect of heat treatment can be studied and optimised. This will be the target of future work.

5. Conclusions

Exploratory tests on welding suitability of an austenitic stainless high manganese steel in similar and dissimilar joints have been carried out. The results show a general suitability delivering crack-free welds in thin gauge sheet material. For square butt welds the mechanical properties still have to be improved. Similar welds break in the fused zone through weakening of the material by the cast structure at the strength of the solution treated material. In the combination with the austenitic stainless steel the strength is determined by the weaker partner 1.4301. Fracture behaviour of the combination with the press hardened martensitic stainless steel 1.4034 is more complicated. Failure is initiated at the fusion line but the crack propagates into the strong base material of 1.4034. All fused zones solidify austenitic with martensitic streaks in regions with increased carbon content. Especially in the last case the results show the necessity of weld heat treatment in order to homogenise or to temper the heat-affected zone in the martensitic steel. The results are not ready for application yet but show promising opportunities. Understanding the complex metallurgy as well as the resulting mechanical behaviour of the welds and utilising them for the production of reliably strong joints by fusion welding will help to enable new constructions for eco-efficient applications.

References

Behm, V., Höfemann, M., Hatscher, A., Springer, A.: Investigations on laser beam welding dissimilar material combinations of a ustenitic high manganese (FeMn) and ferrite steels*, Physics Procedia* 56 (2014), 610-619

Bouaziz, O., Allain, S., Scott, C.P., Cugy, P., Barbier, D., 2011: High manganese austenitic twinning induced plasticity steels: A review of the microstructure properties relationships. *Current Opinion in Solid State and Materials Science* 15, p. 141–168

Dahmen, M., Daamen, M., Hirt, G. 2014: Laser beam welding of high manganese TWIP steels produced by twin roll strip casting. Extended abstract: 2nd International Conference on High Manganese Steel, August 31 - September 4, 2014, Aachen, Germany

Dahmen, M., Janzen, V., Lindner, S., Wagener, R.. 2015a: *Untersuchungen zum Schmelzschweißen höchstfester nichtrostender Stähle mit martensitischem Gefüge mittels Laserstrahl- und MAG-Schweißen*. Forschung für die Praxis P905, Düsseldorf, p. 51

Dahmen, M., Lindner, S., Monfort, D., Petring, D., 2016: Weld metallurgy and mechanical properties of high-manganese ultra-high strength steel dissimilar welds. *Physics Procedia* 83, p. 344 – 351

Janzen, V., Meschut, G. Dahmen, M., Poprawe, R., Lindner, S., Wagener, R., Melz. T., 2015: Investigation on joint characteristics of laser beam welded press hardenable ultrahigh strength steels with ferritic-martensitic and martensitic microstructure, *Welding in the World*, DOI 10.1007/s40194-015-0229-0

Klueh, R.L., Masiaz, P.J., Lee, E.H., 1988. Manganese as an austenite sabilizer in Fe-Cr-Mn-C steels. *Materials Science and Engineering A* 102, 115-124

Lan, P, Zhang, J., 2016. Thermophysical properties and solidification defects of Fe–22Mn–0.7CTWIP Steel. *Steel Research International 87 (2), 250 – 261*

Lee, S., Lee, C., Lee, Y., 2015. Schaeffler diagram for high Mn steels. *Journal of Alloys and Compounds*, 628, 46 – 49

Lindner, S., 2014: Joining processing advices of new Manganese-Chromium steels with high strength and without nickel for automotive-typical joining combinations, *Proceedings of the 4th International Conference on Steels in Cars and Trucks*, June 15 – 19, 2014, Braunschweig, Germany, pp. 375 – 382

Lindner, S., Gerhards, B., Dahmen, M.: Alloyed ultra-high strength steels - Properties, benefits and challenges with laser beam welding, *Laser Technik Journal* (2015), February issue, pp. 48 – 52

Mazancová, E., Ružiak, I., Schindler, I., 2012. Influence of rolling conditions and aging process on mechanical properties of high manganese steels. *Archives of Civil and Mechanical Engineering* 2, 142–14

Mújica, L., Weber, S., Thomy, C., Vollertsen, F., 2009: Microstructure and mechanical properties of laser welded austenitic high manganese steels, *Science and Technology of Welding and Joining* 14(6), p. 517-522

Mújica, L. Weber, S., Pinto, H., Thomy, C., Vollertsen, F.: Microstructure and mechanical properties of laser-welded joints of TWIP and TRIP steels", *Materials Science and Engineering* A527 (2010), 2071–2078

Rossini, M., Russo Spena, P. Cortese, L., Matteis, P., Firrao, D., 2015: Investigation on dissimilar laser welding of advanced high strength steel sheets for the automotive industry", *Materials Science & Engineering* A628, p. 288-296